Journal of Applied Polymer Science

Cellulose Fibers from Cellulose/1-Ethyl-3-Methylimidazolium Acetate Solution by Wet Spinning with Increasing Spinning Speeds

Xiaojun Li,[1,2] Nianke Li,[2] Jigang Xu,[2] Xianquan Duan,[2] Yushan Sun,[2] Qiang Zhao[1,2]

[1]Textile College, Donghua University, Shanghai 201620, People's Republic of China

[2]State Key Laboratory of Biobased Fiber Manufacturing Technology, China Textile Academy, Beijing 100025, People's Republic of China

Correspondence to: X. Li (E-mail: junlx@mail.dhu.edu.cn)

ABSTRACT: Cellulose fibers from cellulose/1-ethyl-3-methylimidazolium acetate solution were prepared by wet spinning with increasing extrusion speeds and draw ratios. The effects of spinning speeds on the structures and mechanical properties of these fibers were investigated by using scanning electron microscopy, wide angle X-ray diffraction, birefringence, thermogravimetric analysis, tensile-fineness tester, and wet friction. The results showed that the crystallinity, orientation, and mechanical properties of the fibers were improved with increasing draw ratio. The break draw ratios, degrees of crystallinity and orientation, tenacities, and wet friction time of the cellulose fibers decreased with increasing extruding speeds. The wet friction time decreased with increasing draw ratio and decreased faster under higher extrusion speed. Due to the high dope concentration and the increased draw ratio, the maximum tenacity of the regenerated cellulose fibers reached 2.73 cN/dtex. © 2013 Wiley Periodicals, Inc. J. Appl. Polym. Sci. **2014**, *131*, 40225.

KEYWORDS: cellulose and other wood products; fibers; ionic liquids; structure-property relations; properties and characterization

Received 1 July 2013; accepted 23 November 2013

DOI: 10.1002/app.40225

INTRODUCTION

Cellulose is the most abundant renewable organic resource on earth and currently regarded as a promising alternative to fossil resources. However, lack of thermal and solution processability of cellulose due to the strong intermolecular and intramolecular hydrogen bonding greatly restricts its further development and utilization.[1,2] For more than one century, great efforts have been devoted to the development of effective solvents for cellulose.[2] Until now, only the viscose process, cuprammonium hydroxide process and N-methylmorpholine-N-oxide (NMMO) process have been industrialized to produce regenerated cellulose fibers. However, both the viscose and the cuprammonium rayon process produce highly toxic by-product waste and pollutants.[3] The instability of NMMO may cause consumption of the expensive solvent and bring a safety risk; in addition, fibers from NMMO are easy to fibrillate,[3] which greatly restricts their application.

However, a new class of solvents was opened to the cellulose research community when Swatloski et al.[4] reported the use of ionic liquids as solvents for cellulose in 2002. Ionic liquids are a series of organic salts with the melting points below 100°C. Due to their nonvolatility, controllable physical properties, stable chemical properties, ionic liquids have attracted widespread attentions in recent years.[5] Most ionic liquids can be easily recycled, which make them suitable for use as solvents.[5] It has been proven that some of the ionic liquids with a imidazole ring could directly dissolve cellulose in similar processes to that of NMMO, such as 1-butyl-3-methylimidazolium chloride ([BMIM]Cl),[6,7] 1-alkyl-3-methylimidazolium chloride,[8] 1-ethyl-3-methylimidazolium chloride,[9] 1-ethyl-3-methylimidazolium acetate ([EMIM]Ac),[10] and 1-ethyl-3-methylimidazolium diethyl phosphate.[11] Among ionic liquids with the imidazole ring mentioned above, [EMIM]Ac has comparatively low melting point and can dissolve cellulose up to 25 wt %,[12] indicating high efficiency in cellulose dissolution and shaping processes. Compared with chloride anion, the acetate anion of [EMIM]Ac shows low toxicity.[2,13] All these proved that [EMIM]Ac is a promising solvent for the manufacture of regenerated cellulose fibers.

There have been many reports in the literature of the solubilities[14–25] and rheological properties[26–32] of the cellulose solution in ionic liquids, but few about the spinning process[33–35] and especially about the wet spinning process of cellulose/[EMIM]Ac solution.[36,37] By wet spinning of cellulose from [EMIM]Ac into hot water without drawing, Olsson and Westman[36] prepared fibers of different mechanical qualities, and showed that both tenacity and stiffness increased steeply with increased degree of polymerization of the polymers. The work of Ingildeev et al.[37] indicated that cellulose fibers, wet spun from a 6 wt % cellulose

solution in [EMIM]Ac, displayed the lowest fibrillation tendency compared with those from [EMIM]Ac or NMMO by dry wet spinning. The good spinnability of cellulose/[EMIM]Ac solution in wet spinning and the low fibrillation tendency of the regenerated cellulose fibers make [EMIM]Ac different from NMMO and other ionic liquids in the spinning process and the following products, and also lead to more expectation of practical application of [EMIM]Ac for regenerating cellulose fibers.

Although regenerated cellulose fibers had been successively wet spun from [EMIM]Ac, the mechanical properties of these fibers were not satisfactory.[36,37] Some of the challenges might come from the distinctive spinning process different from the traditional wet spinning process. The structure and properties of traditional wet spun fibers, such as polyacrylonitrile, polyvinyl chloride, and polyvinyl alcohol, could be greatly improved by developing their crystallinity and orientation in the coagulating bath and subsequent multi-step drawing processes.[38] However, this is not the case for cellulose due to its strong hydrogen bonding interactions during coagulation. The structure and properties of regenerated cellulose fibers from direct solvents, such as NMMO, [BMIM]Cl, and [EMIM]Ac, were mainly determined in the first drawing and coagulating stage,[6,9] after which the structures of fibers were fixed so tightly that they did not stand any effective stretching between the godets. So far, the influence of spinning speeds and coagulation conditions on structures and properties of the fibers wet spun from cellulose/[EMIM]Ac solution was still unclear. More detailed studies of the wet spinning process of cellulose/[EMIM]Ac solution needed to be performed. In this article, wet spinning of cellulose in [EMIM]Ac with increasing extrusion and draw speeds was performed. For comparison, the coagulation conditions remained unchanged. The regenerated cellulose fibers were subsequently characterized by various methods. On the basis of these results, the effects of the extrusion and drawing speeds on the structures and properties of the final cellulose fibers were discussed.

EXPERIMENTAL

Materials

[EMIM]Ac synthesized and purified in our laboratory according to references,[5,39,40] with the purity ≥98.0%, was used as the solvent. Bleached kraft dissolving softwood pulps (DP 525 with an α-cellulose content of 98%), were supplied by Xinxiang Chemical Fibers Plant. The pulp sheets were cut into small pieces, and pulverized to be powders with their length less than 1 mm. [EMIM]Ac and the pulp were dried at 60°C under vacuum for 12 h before use.

Dissolving and Spinning

The cellulose solution was prepared by first mixing dry cellulose with [EMIM]Ac at room temperature, and then heating the mixtures under vacuum at 100°C for 5 h. The weight of [EMIM]Ac was 350 g. The concentration of cellulose in solution was 12 wt %. The dissolving process was performed in a stainless steel cylinder. To check whether the pulps were totally dissolved, samples were taken from the dissolving mixture and observed with Polarizing Microscopy (POM).

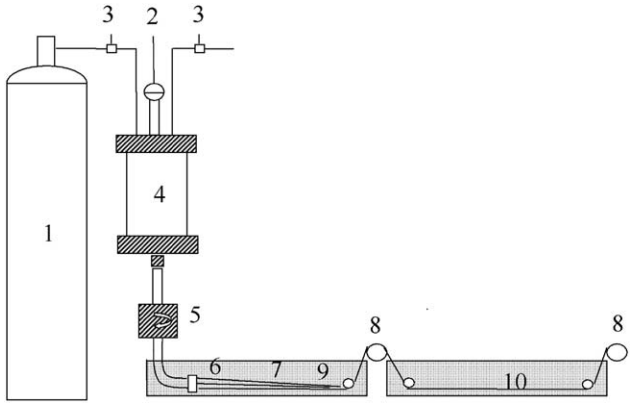

Figure 1. Schematic diagram of dissolving and spinning process: (1) nitrogen cylinder, (2) pressure gage, (3) needle valve, (4) dissolving kettle, (5) metering pump, (6) spinneret, (7) filaments, (8) godet roller, (9) coagulation bath, (10) washing bath.

After dissolution, the solution was transferred under N_2 pressure of 8 kgf to the metering pump, and then pumped through the heating trunk and a 300-hole spinneret into the coagulation bath. Fibers out of the coagulation bath were immediately dipped into a washing bath and then rolled up. To remove any remnant of solvent, the fibers were immersed in pure water at room temperature for five times, 2 h each. Figure 1 shows the diagram of the spinning process. The coagulating bath was composed of water and [EMIM]Ac (90 wt/10 wt). An appropriate amount of [EMIM]Ac in the coagulation bath might help to increase the deformability of the extruded filaments. The temperature of the coagulation bath was kept at 28 ± 1°C. The winding speed was changed with the extrusion speed. For each extrusion condition, the maximum winding speed was recorded, as shown in Table I. The cellulose fibers prepared with the draw ratio toward and close to the break draw ratio were collected as samples, as shown in Table II.

Scanning Electron Microscopy (SEM)

Scanning electron microscopy (JEOL, JSM-6360) was used to observe the cross sections and surfaces of the cellulose fibers. The sample surfaces were coated with gold in a Polaron E5100 sputter coater (Polaron Equipment, England) to enhance electrical conductivity. The operating voltage of the microscope was 10 kV.

Birefringence (Δn)

A polarized light microscope (Laborlux 12 POL, Leitz, Wetzlar, Germany) equipped with a Berek compensator was used to measure the birefringences of the cellulose fibers. For each sample, the average value of 10 tests was recorded as the final birefringence of the cellulose fibers.

Wide Angle X-ray Diffraction (WAXD)

Wide angle X-ray diffraction measurements were performed on an X'Pert PRO diffractometer from Panalytical. The diffractometer was equipped with a CuKa source. The copper radiation consists in two radiations at $k_1 = 1.540598$ Å and $k_2 = 1.544426$ Å. The radiation was generated with a 40 mA current and a 40 kV voltage, and filtered with a Ni filter plate. After the cellulose fibers were finely bonded on the specimen holder, equatorial

Table I. Spinning Speeds and Draw Ratios of Samples Obtained

Extrusion speed ($m \cdot min^{-1}$)	Break draw speed ($m \cdot min^{-1}$)	Break draw ratio
0.29	0.97	3.32
0.43	1.22	2.81
0.63	1.41	2.24

scans were conducted by steps of 0.05° ranging from 5 to 60°, and azimuthal scans were conducted by steps of 0.5° ranging from 90 to 270° under (020) orthorhombic reflections.

Crystallinity was calculated from the following equation[41]:

$$Cr(\%) = \frac{A_c}{A_c + A_a} \times 100\% \quad (1)$$

Where Cr is crystallinity, A_c is the area of all crystalline peaks, A_a is the area of amorphous region. The crystallization index was calculated from the Segal equation[41]:

$$CrI = \frac{I_{hkl} - I_{am}}{I_{hkl}} \times 100 \quad (2)$$

where CrI is crystallization index, for cellulose I: I_{hkl} is the intensity of (020) reflection, I_{am} is the intensity of $2\theta = 18°$, for cellulose II: I_{hkl} is the intensity of $(1\bar{1}0)$ reflection, I_{am} is the minimum intensity between peaks of (110) and $(1\bar{1}0)$ reflections.

The apparent crystal sizes along three lattice directions (perpendicular to the diffracting planes) were calculated from Scherrer equation[41]:

$$L_{hkl} = \frac{K\lambda}{\beta \cos\theta} \quad (3)$$

Where L_{hkl} is the size of a crystallite perpendicular to its diffracting plane, K is Scherrer constant of 0.9, λ is the wavelength of the X-rays of 0.154 nm, β is the full-width at half maximum (FWHM) of the corresponding (hkl) reflection peak in radians.

The Herman crystalline orientation factor (f_x) was calculated from eqs. (4) and (5)[41,42]:

$$f_x = \frac{1}{2}\left[3 < \cos^2\varphi > -1\right] \quad (4)$$

$$< \cos^2\varphi > = \frac{\int_0^{\pi/2} I(\varphi)\cos^2\varphi \sin\varphi d\varphi}{\int_0^{\pi/2} I(\varphi)\sin\varphi d\varphi} \quad (5)$$

According to widely approved viewpoints, fibers are composed of crystalline and amorphous regions and birefringences have the additive property, the amorphous orientation factor could be calculated from eq. (6)[43]:

$$f_a = \left(\frac{\Delta n}{0.0545} - \alpha f_x\right)\frac{1}{1-\alpha} \quad (6)$$

Where Δn is the birefringence of the cellulose fibers measured, α is the crystallinity of the cellulose fibers measured, f_a is the amorphous orientation factor.

Thermogravimetric Analysis (TGA)

Thermogravimetric analysis was performed using a Perkin Elmer Pyris 1 TGA instrument. In each analysis, 4 mg of previously milled cellulosic fibers were heated at a rate of 20°C min^{-1} from 28 to 600°C under N_2 atmosphere (20 $mL \cdot min^{-1}$).

Mechanical Properties

Fineness, tenacities, breaking strains and moduli of the regenerated cellulose fibers were tested by XD-1 Fineness Tester and XQ-1 Tensile Tester, respectively. The gauge length was 20 mm and the constant rate of elongation was 20 $mm \cdot min^{-1}$. For each sample, the average value of 20 measurements was recorded as the final test result.

Wet Friction Time

Wet friction time of fibers was obtained by recording the friction time of samples on a rotating roller covered with wet cotton cloth until breakage.[44] Figure 2 is the schematic diagram. The diameter of roller was 12 cm, the line speed of the roller surface was 4 $m \cdot min^{-1}$, and the weight was 27 g. For comparison, the lengths and weights of all samples tested were kept to be 30 cm and 0.0200 ± 0.0005 g, respectively. For each sample, the average value of three measurements was recorded as the test result.

RESULTS AND DISCUSSION

Spinning Process Analysis

By wet spinning of cellulose/[EMIM]Ac solution with the concentration of 12 wt %, the cellulose fibers were successfully prepared at various extrusion and draw speeds. For each extrusion speed, the break draw speed and break draw ratio were obtained and shown in Table I. The break draw ratios were typically used to characterize the spinnability of the solution. The biggest break draw ratio of the spinning solution reached 3.32, indicating excellent drawability of the solution. With the increment of extrusion speed, the break draw speed also increased, but the break draw ratio and the highest attainable draw ratio decreased, implying decreasing spinnability. Greater extrusion speeds gave larger internal stress in the extruded filaments, which need more time to relax. Ordinarily, more relaxation time meant lower rate of deformation and smaller break draw ratio. The phenomenon appearing in this study was in accord with this deduction.

Table II. Break Draw Speeds and Break Draw Ratios of Cellulose/[EMIM]Ac Solution with Different Extrusion Speeds

Samples No.	1	2	3	4	5	6	7	8	9	10
Extrusion speed ($m \cdot min^{-1}$)	0.29	0.29	0.29	0.29	0.43	0.43	0.43	0.63	0.63	0.63
Drawing speed ($m \cdot min^{-1}$)	0.38	0.56	0.75	0.92	0.92	1.03	1.14	1.13	1.24	1.36
Drawing ratio	1.3	1.94	2.59	3.17	2.12	2.38	2.63	1.79	1.97	2.17

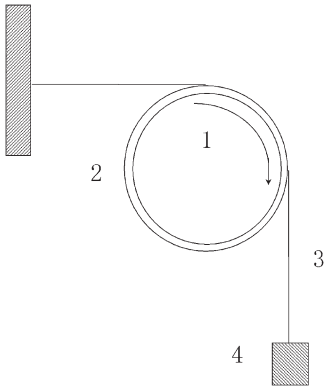

Figure 2. Schematic diagram of wet friction process: (1) roller, (2) wet cotton cloth, (3) a bunch of filaments, (4) weight.

SEM Analysis

Figure 3 presents the SEM micrographs of cross section and lateral surface of the regenerated cellulose fiber. All SEM micrographs of the fiber samples look similar. The samples cut by scissor gave smooth lateral surfaces, round, compact, and uniform cross sections, whereas those broken under liquid nitrogen gave granular cross sections. A porous structure or sheath-core structure usually appeared in wet-spun fibers as a result of phase separation accompanied by volume changes. Nevertheless, no obvious holes and sheath-core structure could be observed from the SEM micrographs. It is probably due to the fact that the sizes of the voids and the thickness of the sheath in the regenerated cellulose fibers are in nanometers, as is the case for Lyocell fibers from NMMO by dry–wet spinning.[45]

Degree of Crystallinity and Crystal Size

To calculate the degrees of crystallinity and crystal sizes of the cellulose fibers, curve fitting was used to separate the different crystalline peaks and amorphous region. The method is to subtract a region tangent to the whole virgin curve as the amorphous region, and then to resolve the crystalline region by using the PEAKFIT software, as shown in Figures 4 and 5. For comparison, the peaks of (11(—)0) and (020) reflections were set at $2\theta = 20.1$ and 21.8°, respectively.[46] The r^2 values of all fittings were more than 99.6%.

The parameters calculated above are shown in Table III. It can be seen that the *CrI*, *Cr*, and crystal size of all samples are close to each other. In solution-spinning, the important structural characteristics of as-spun fibers regarding their crystalline texture are not so sensitive to spinning conditions as that in melt-spinning.[38] However, the regular changes of *CrI*, *Cr*, and crystal size with the increment of draw ratio can be found in Figure 6 and Table III. For samples with the same extruding speed, the *CrI* and *Cr* increased to peak values and then decreased with increasing draw ratio, but the crystal size increased monotonically with increasing draw ratio under low extrusion speeds

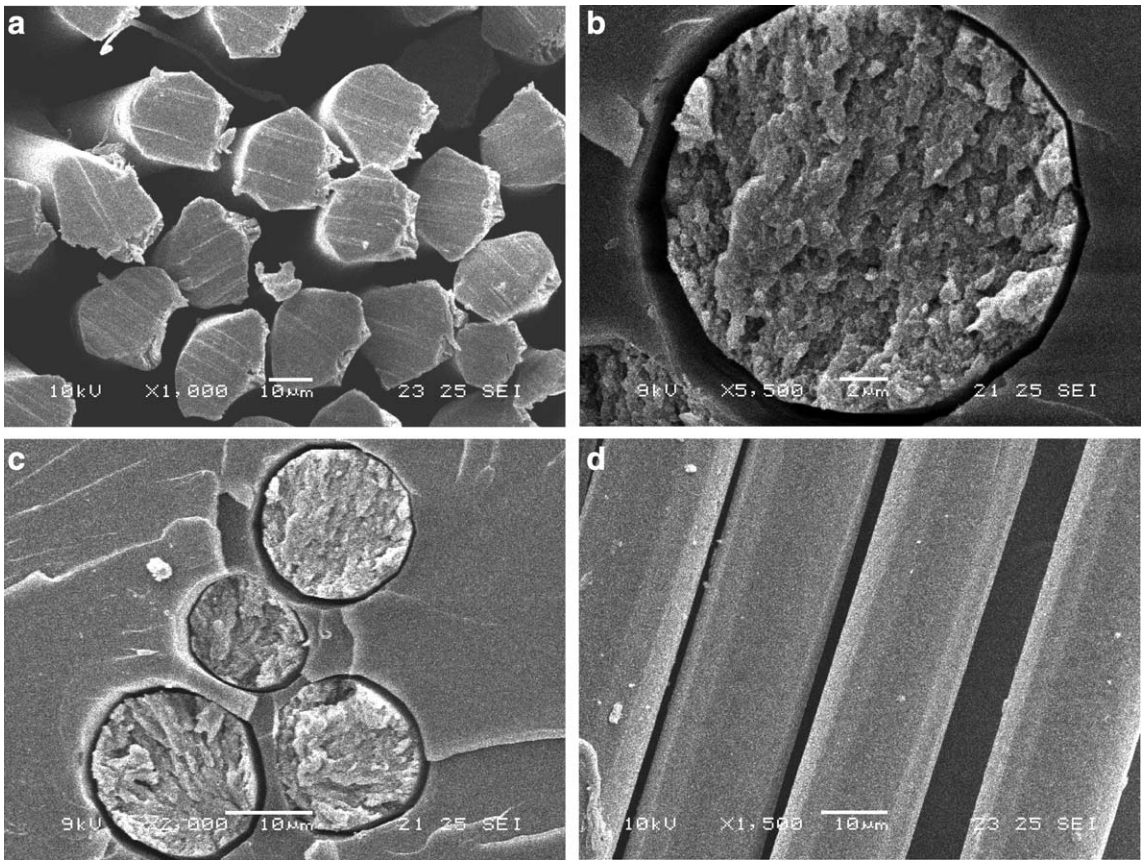

Figure 3. Scanning electron micrograph of regenerated cellulose fiber, (a) cross section cut by scissor, ×1000, (b) and (c) cross section of paraffin-embedded fiber after cooled by liquid nitrogen, ×5500 and ×2000, (d) lateral surface, ×1500.

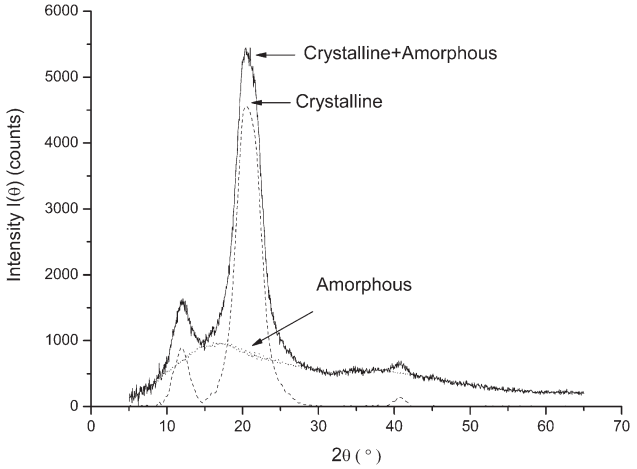

Figure 4. Subtracting a region tangent to the virgin curve as the amorphous region.

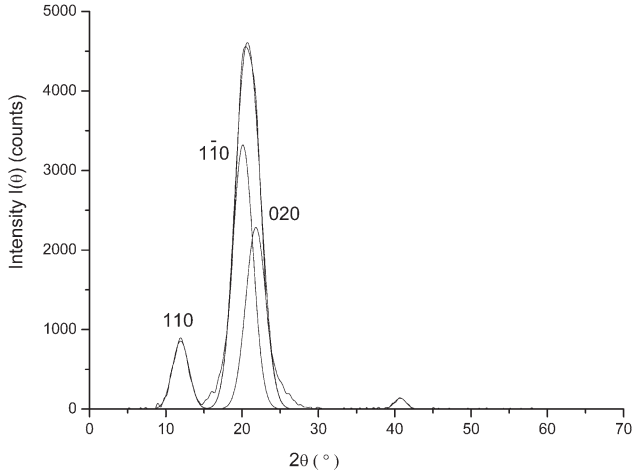

Figure 5. Peak resolution of crystalline region after subtracting the amorphous region.

(Samples 1–7). It can be explained that, stress-induced crystallization could be enhanced by increasing draw stress derived from increasing draw ratio, and thus promoted the increase of crystallinity and the growth of crystal size in the spinline. The decrease of crystallinity after reaching a peak value seemed to imply an excessive drawing which might do harm to the crystallization and the formation of a dense structure in the spinline.

Figure 6 also illustrates the regular changes of crystalline texture with the increment of extrusion speed, such as: (1) With the increment of extrusion speed, the maximum crystallinity for each extrusion speed decreased, but the corresponding draw ratio seemed to increase at first (Samples 5–7) and then decreased (Samples 8–10); (2) The change rate of the crystallinity increased and the curves became sharp and steep with increasing extrusion speed; (3) The excessive drawing, implied by the decrease of crystallinity after reaching a peak value with increasing draw ratio, decreased and tended to vanish with increasing extrusion speeds.

In wet spinning, the coagulation, orientation, and crystallization synchronously proceed from the surface to the center of the filaments, meanwhile, a rigid "skin" forms, develops and transmits most of the spinline stress composed of the internal stress and the draw stress.[47] In the region close to the spinneret where the skin is thin, the internal stress perpendicular to the drawing direction impedes the orientation of the extruded filaments, whereas the draw stress induces high deformation, orientation and hence the orientation-induced crystallization. As the extrusion speed increased, the internal stress increased and the drawing stress decreased,[47] because the stress tolerance of the skin remained unchanged under the same coagulation condition. The above mentioned decrease of crystallinity with increasing extrusion speed should be mainly ascribed to the increasing internal stress and decreasing draw stress.

The increase of the draw ratio corresponding to the maximum crystallinity (of Samples 2 and 6) for each extrusion speed should be attributed to the increasing deformability of spinning line near the spinneret, whereas the decrease of the draw ratio corresponding to the maximum crystallinity (of Samples 6 and 10) for each extrusion speed should be ascribed to the decrease of draw stress. The increasing change rate of the crystallinity and the even steeper curves should be mainly ascribed to both the increasing deformability and the decreasing draw stress.[47] With the further increment of the extrusion speed (of Samples 8–10), the draw stress decreased to such a degree that it could

Table III. Crystallization Index, Crystallinity, Crystal Sizes, and Orientation of the Regenerated Cellulose Fibers

#	CrI (%)	Cr (%)	L_{110} (nm)	$L_{1\bar{1}0}$ (nm)	L_{020} (nm)	Δn	f_x	f_a	f
1	82.26	40.78	3.175	2.726	2.757	0.0367	0.458	0.822	0.673
2	85.03	44.06	3.072	2.862	2.786	0.0374	0.569	0.779	0.686
3	83.90	43.50	3.150	2.837	2.883	0.0392	0.570	0.834	0.719
4	82.59	41.70	3.318	2.861	2.963	0.0380	0.589	0.775	0.697
5	81.69	40.02	3.387	2.794	2.944	0.0377	0.565	0.776	0.692
6	84.22	43.44	3.509	2.726	2.892	0.0381	0.570	0.798	0.699
7	84.09	43.1	3.529	2.899	2.957	0.0356	0.532	0.745	0.653
8	80.70	38.28	3.376	2.735	2.848	0.0354	0.550	0.711	0.650
9	83.72	42.50	3.192	2.801	2.801	0.0370	0.563	0.765	0.679
10	83.94	42.81	3.243	2.784	2.863	0.0366	0.560	0.756	0.672

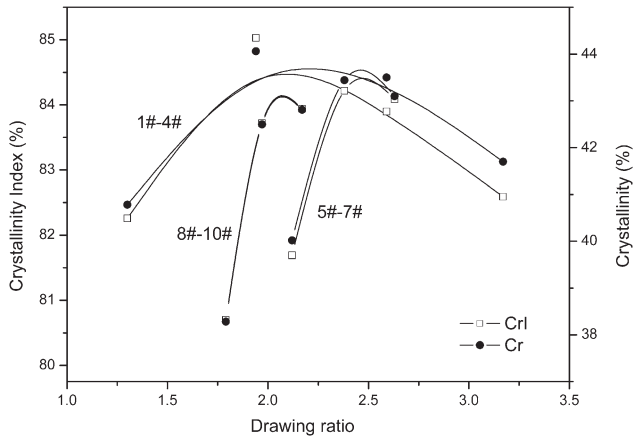

Figure 6. Changes of crystallinity index (CRI) and crystallinity (CR) of samples with different extrusion speeds and increasing draw ratio.

not induce the crystal sizes to continue their increase or the crystallinity to decrease after reaching the peak value. Consequently the excessive drawing phenomenon vanished. From Table III, it could also be concluded that samples with the medium extrusion speed (Samples 5–7) had the biggest crystal sizes. Under the same coagulating condition, the proper extruding and draw speed made the crystallization process and the coagulating process well-matched, and therefore gave the biggest crystal sizes.

Degree of Orientation

Birefringence and X-ray methods can effectively characterize the orientation of small areas such as chain segments in a polymer. So measurements of birefringences and azimuthal WAXD scans under (020) reflection at $2\theta = 21.8°$ were used to determine the degrees of orientation of the cellulose fibers.

Figure 7 shows the accumulative azimuth scanning curves with unified baselines. The higher height corresponds to less FWHM of the peak, which reveals the relatively higher orientation. The orientation parameters measured and calculated are shown in Table III.

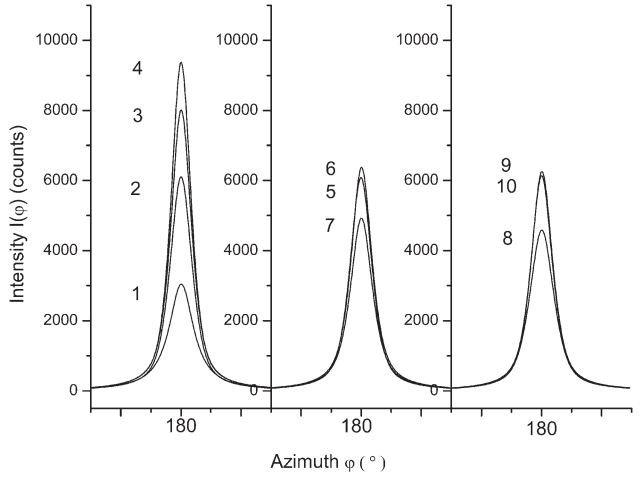

Figure 7. Accumulative azimuth scanning curves with unified baselines of Sample 1–10.

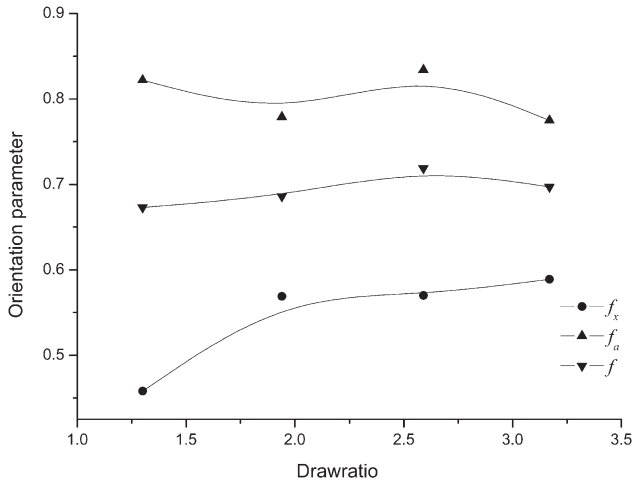

Figure 8. Changes of orientation parameters with increasing draw ratio of Sample 1–4.

Figure 8 shows the changes of orientation parameters with draw ratio for Samples 1–4. It's obvious that the process could be divided into three stages.

In the first stage, with the draw ratio increasing from 1.30 to 1.94, f_x increased, whereas f_a decreased (Sample 1–2). By combining the data of orientations with those of crystallinities, it might be deduced that a higher draw ratio was accompanied by greater deformation rate and drawing force, which broke the initial order of chain segments in amorphous regions and led to the decrease in f_a. With the help of the drawing force, some amorphous regions oriented and transformed into crystalline regions, which promoted the crystallization and the crystalline orientation (Sample 1–2). Although the orientation of amorphous regions decreased, the total orientation increased.

In the second stage, the amorphous orientation began to increase only after most of the crystallization process had finished (Sample 2–3). Chain segments in the amorphous region oriented further, but the orientation in crystalline regions approximately stayed the same. The total orientation kept increasing.

In the third stage, when excessive drawing was applied, the amorphous orientation decreased again and the crystalline orientation increased slightly (Sample 4). The change in this stage implied that some internal fracture, disorientation, and reorientation had happened in amorphous regions.

For Samples 5–10, changes of orientation parameters with draw ratio are shown in Figure 9 and seem to be identical with the latter two stages of Samples 1–4. The amplitudes of variation of amorphous orientations were larger than those of crystalline orientations. By comparing the orientation parameters of all samples of the three extrusion speeds, it could be concluded that the maximum degree of orientation and its corresponding draw ratio for each extrusion condition decreased with the increase in extrusion speed. The mechanism might be that, the filaments extruded from the spinneret orifice with higher extruding speed had greater internal stress, which weakened the orientation along drawing direction. As a whole, the change

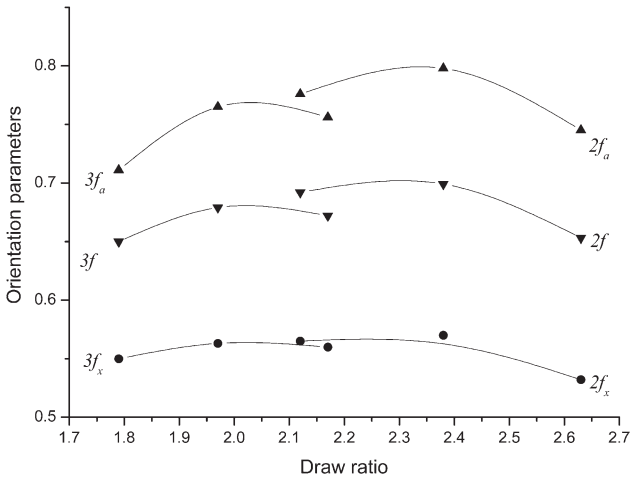

Figure 9. Changes of orientation parameters with increasing draw ratio of Sample 5–10, $2f_a$, $2f$, $2f_c$ represent the f_a, f, f_c of Sample 5–7, respectively, $3f_a$, $3f$, $3f_c$ represent those of Sample 8–10.

trends of orientation matched that of crystallinity for all samples, except that the draw ratio for the maximum orientation was higher than that for the maximum crystallinity of Samples 1–4. It implied that, under a sufficient coagulation condition, the excessive drawing first brought the decrease of crystallinity and then of the orientation.

TGA Analysis

The TGA profiles of raw cellulose, Samples 1 and 3 are displayed in Figure 10. It indicates that the weight losses of all samples mainly happened at about 100 and 360°C. The former loss should be ascribed to the loss of moisture absorbed in the samples, the latter weight loss at about 360°C should be related to the degradation of cellulose. By comparing TGA profiles of raw cellulose and regenerated cellulose fibers, the regenerated cellulose fibers had higher moisture absorption, a lower degradation temperature, and more residue carbon than raw cellulose. This was most likely due to the relatively low densities of the crystalline and amorphous region of regenerated cellulose, the possible loose structure resulting from mass-transfer phenomena in wet spinning process of regenerated cellulose, and

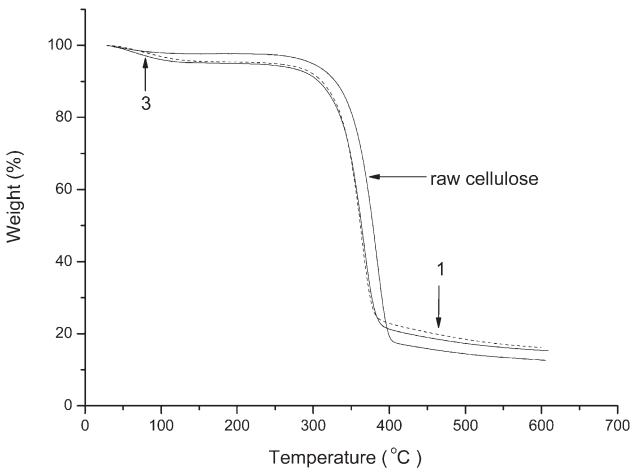

Figure 10. TGA profiles of raw cellulose, Sample 1 and 3.

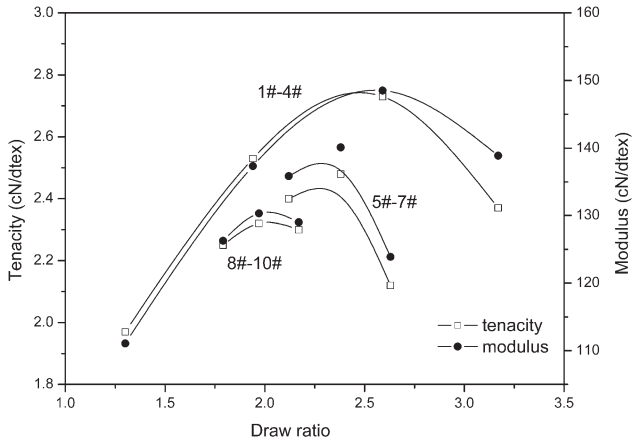

Figure 11. Changes of tenacity and modulus of all samples with increasing draw ratio.

the high thermodynamic stability of cellulose II compared with cellulose I. Figure 10 also displays less moisture loss and more residue of Sample 1 than Sample 3, indicating relatively more internal surface area appeared in Sample 3. This is probably due to the increase in number and smaller dimension of the voids with increasing draw ratio and stress. The detailed mechanism might be further revealed by the structure and distribution of the internal voids, which are still under investigation.

Mechanical Properties

Figures 11–13 show the relationship between the draw ratios and the mechanical properties of the samples with different extruding speeds. With the increment of draw ratio, the tenacity and modulus of all the cellulose fibers with different extrusion speeds increased to a maximum and then decreased, as shown in Figure 11. With the increases in the extruding speeds, the tenacity, modulus, and the peak values and their corresponding draw ratios decreased. By comparing Figures 6, 8, and 9, it could be found that trends of the tenacity and modulus were accordant with that of the degrees of amorphous orientation except Samples 1–2. Generally, tenacity and modulus were directly related to the amorphous orientation of fibers. The

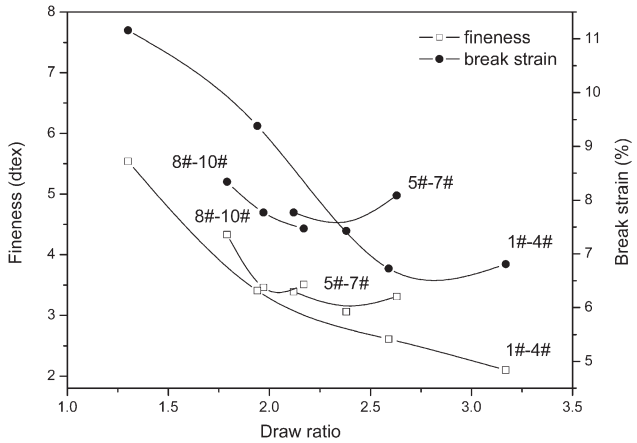

Figure 12. Relationship between finenesses and break strains of the cellulose fibers with increasing draw ratio.

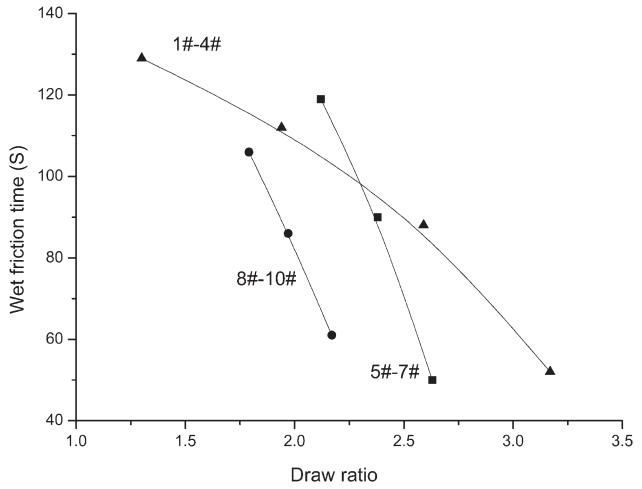

Figure 13. Changes of wet friction time of all samples with increasing draw ratio.

deviation might be ascribed to the increase in the number of tie molecules[48] with increasing draw ratio and crystallinity.

When the draw ratio was close to the break draw ratio, excessive drawing brought a decrease of crystallinity and orientation. In other words, the increase of internal fracture or structural defects decreases the mechanical properties of cellulose fibers. Compared with the fibers wet spun by Olsson and Westman[36] and Ingildeev et al.,[37] the mechanical properties of regenerated cellulosic fibers has been improved, which might be mainly attributed to the high concentration of cellulose and the increased draw ratio.

Figure 12 gives the relationship between fineness and break strains of the cellulose fibers. With the increase in draw ratio, both fineness and break strains of the cellulose fibers decreased and had similar shape of curves. All the curves have to some extent a concave curvature at the draw ratio near the break draw ratio, which were clear for samples with higher extruding speeds. The reason might be the greater contraction of the looser structures of Samples 4, 7, and 10, which probably originated from the internal fracture or defects as mentioned above.

Figure 13 gives the relationship between the draw ratio and wet friction time of all samples. With increasing draw speeds, wet friction time of the corresponding samples decreased. Larger draw ratios gave fibers higher degrees of crystallinity and orientation, but left the fibers with weaker cohesive forces along the radius, and therefore made the cellulose fibers easy to fibrillate and break under wet friction. For those with higher extrusion speeds, their wet friction time decreased faster, indicating greater influence of draw ratio on the structure formation of the cellulose fibers under higher extruding speeds. This trend was similar to that of crystallinity shown in Figure 9, implying the induction or promotion effects of crystallization and orientation on the fibrillation of cellulose fibers.

CONCLUSIONS

Smooth, compact cellulose fibers were regenerated from cellulose/[EMIM]Ac (12 wt %) solutions by wet spinning. Due to the high concentration of cellulose in [EMIM]Ac and the increased draw ratio, the crystallinity, orientation and mechanical properties of the fibers were improved, the maximum tenacity of the regenerated cellulose fibers reached 2.73 cN/dtex. Extrusion speed should be carefully chosen because increasing extrusion speed might decrease the spinnability of the dope, and worsen the mechanical properties of the fibers. Both the increments of the extrusion and draw speeds increased the fibrillation tendency of regenerated cellulose fibers. Other factors are still under investigation. With the further research of the wet spinning process of cellulose/[EMIM]Ac solution, cellulose fibers with higher tenacity and lower fibrillation tendency can be expected.

ACKNOWLEDGMENTS

This study was supported by grant from Major State Basic Research Development Program of China (grant number: 2012CB724610).

REFERENCES

1. Wang, P. Q.; Su, M. R.; Zhu, Y. Q.; Tang, L. G.; Gao, J.; Yang, Z. L.; Wu, Y. M.; Tai, D. S. In Cellulose Science; Gao, J., Tang, L. G., Eds.; Science Press: Beijing, **1996**; Chapter *1*, p 1.
2. Liebert, T. In Cellulose Solvents: For Analysis, Shaping and Chemical Modification; Tim, F. L., Thomas, J. H., Kevin, J. E., Eds.; American Chemical Society: **2010**; p 3.
3. Cuculo, J. A.; Aminuddin, N.; Frey, M. W. In Structure Formation in Polymeric Fibers; Salem, D. R., Ed.; Hanser Publishers: Munich, **2000**; p 296.
4. Swatloski, R. P.; Spear, S. K.; Holbrey, J. D.; Rogers, R. D. *J. Am. Chem. Soc.* **2002**, *124*, 4974.
5. Pinkert, A.; Marsh, K. N.; Pang, S.; Staiger, M. P. *Chem. Rev.* **2009**, *109*, 6712.
6. Bentivoglio, G.; Roder, T.; Fasching, M.; Buchberger, M.; Schottenberger, H.; Sixta, H. *Lenz. Ber.* **2006**, *86*, 154.
7. Remsing, R. C.; Swatloski, R. P.; Rogers, R. D.; Moyna, G. *Chem. Commun.* **2006**, *12*, 1271.
8. Zhang, H.; Wu, J.; Zhang, J.; He, *J. Macromolecules* **2005**, *38*, 8272.
9. Kosan, B.; Michels, C.; Meister, F. *Cellulose* **2008**, *15*, 59.
10. Li, D.; Li, K.; Ma, Y.; Gong, G.; Wang, S. *Synth. Fiber China* **2007**, *2*, 28.
11. Vitz, J.; Erdmenger, T.; Haensch, C.; Schubert, U. *Green Chem.* **2009**, *11*, 417.
12. Kosan, B.; Schwikal, K.; Meister, F. *Cellulose* **2010**, *17*, 495.
13. Liebert, T.; Heinze, T. *BioResources* **2008**, *3*, 576.
14. Laus, G.; Bentivoglio, G.; Schottenberger, H.; Kahlenberg, V.; Kopacka, H.; Röder, T.; Sixta, H. *Lenz. Ber.* **2005**, *84*, 71.
15. Wan, Z.; Li, L.; Cui, S. *Biopolymers* **2008**, *89*, 1170.
16. Zhang, J.; Zhang, H.; Wu, J.; Zhang, J.; He, J.; Xiang, *J. PCCP* **2010**, *12*, 1941.
17. Liu, Z.; Remsing, R. C.; Moore, P. B.; Moyna, G. *ACS Sym. Ser.* **2007**, *975*, 335.

18. Liu, H.; Sale, K. L.; Holmes, B. M.; Simmons, B. A. *J. Phys. Chem. B* **2010**, *114*, 4293.
19. Xu, A.; Wang, J.; Wang, H. *Green Chem.* **2010**, *12*, 268.
20. Trulove, P. C.; Reichert, W. M.; De Long, H. C.; Klinec, S.; Rahatekard, S.; Gilmane, J.; Muthukumarf, M. *ECS Trans.* **2009**, *16*, 111.
21. Evlampieva, N. P.; Vitz, J.; Schubert, U. S.; Ryumtsev, E. I. *Russ. J. Appl. Chem.* **2009**, *82*, 666.
22. Cuissinat, C.; Navard, P.; Heinze, T. *Carbohyd. Polym.* **2008**, *72*, 590.
23. Gericke, M.; Schlufter, K.; Liebert, T.; Heinze, T.; Budtova, T. *Biomacromolecules* **2009**, *10*, 1188.
24. Dorn, S.; Wendler, F.; Meister, F.; Heinze, T. *Macromol. Mater. Eng.* **2008**, *293*, 907.
25. Heinze, T.; Dorn, S.; Schoebitz, M.; Liebert, T.; Köhler, S.; Meister, F. *Macromol. Symp.* **2008**, *262*, 8.
26. Chen, X.; Zhang, Y.; Cheng, L.; Wang, H. *J. Polym. Environ.* **2009**, *17*, 273.
27. Collier, J. R.; Watson, J. L.; Collier, B. J.; Petrovan, S. *J. Appl. Polym. Sci.* **2009**, *111*, 1019.
28. Kosan, B.; Michels, C.; Meister, F. *Cellulose* **2008**, *15*, 59.
29. Sammons, R. J.; Collier, J. R.; Rials, T. G.; Petrovan, S. *J. Appl. Polym. Sci.* **2008**, *110*, 3203.
30. Sammons, R. J.; Collier, J. R.; Rials, T. G.; Petrovan, S. *J. Appl. Polym. Sci.* **2008**, *110*, 1175.
31. Kuang, Q. L.; Zhao, J. C.; Niu, Y. H.; Zhang, J.; Wang, Z. G. *J. Phys. Chem. B* **2008**, *112*, 10234.
32. Song, H.; Zhang, J.; Niu, Y.; Wang, Z. *J. Phys. Chem. B* **2010**, *114*, 6006.
33. Michels, C.; Kosan, B. *Lenz. Ber.* **2006**, *86*, 144.
34. Cai, T.; Zhang, H.; Guo, Q.; Shao, H.; Hu, X. *J. Appl. Polym. Sci.* **2010**, *115*, 1047.
35. Bentivoglio, G.; Roeder, T.; Fasching, M.; Buchberger, M.; Schottenberger, H.; Sixta, H. *Lenz. Ber.* **2006**, *86*, 154.
36. Olsson, C.; Westman, G. *J. Appl. Polym. Sci.* **2013**, *127*, 4542.
37. Ingildeev, D.; Effenberger, F.; Bredereck, K.; Hermanutz, F. *J. Appl. Polym. Sci.* **2013**, *128*, 4141.
38. Gupta, V. B.; Kothari, V. K. In Manufactured Fibre Technology; Chapman & Hall: London, **1997**; p 134.
39. Wasserscheid, P.; Welton, T., Eds. Ionic Liquids in Synthesis; Wiley–VCH: Weiheim, **2007**; p 7.
40. Xu, J.; Chen, G.; Li, X.; Sun, Y.; Gao, J.; Liu, B. *CN Pat. 101337938 B;* **2012**.
41. Yang, Z. L.; Jiang, T. P.; Wang, Q. R.; Wu, G. M. In Cellulose and Viscose Rayon; Yang, Z. L., Ed.; Textile Industry Press: Beijing, **1980**; Chapter *3*, p 114.
42. Liang, B. R.; Qu, F. Z.; Pan, L. H.; Liu, X. J.; Wu, C. X. In Polymer Physics; Liang, B. R., Ed.; China Textile Press: Beijing, **2000**; Chapter *3*, p 77.
43. Guo, Q.; Cai, T.; Zhang, H.; Shao, H.; Hu, X. *Synth. Fiber China* **2009**, *4*, 20.
44. Guo, J.; Shao, H.; Hu, X.; Shen, Y. *Shanghai Text. Technol.* **2002**, *30*, 51.
45. Fink, H. P.; Weigel, P.; Purz, H. J.; Ganster, *J. Prog. Polym. Sci.* **2001**, *26*, 1473.
46. Oh, S. Y.; Yoo, D. I.; Shin, Y.; Kim, H. C.; Kim, H. Y.; Chung, Y. S.; Park, W. H.; Youk, J. H. *Carbohydr. Res.* **2005**, *340*, 2376.
47. Ziabicki, A. In Fundamentals of Fibre Formation: The Science of Fibre Spinning and Drawing; Wiley: London, **1976**; p 92.
48. Sun, Y. S.; Wu, Z. Q.; Wei, D. Z.; Li, Z. H.; Luo, Q. *China Synth. Fibre Ind.* **1988**, *11*, 32.